

Free-form Design of Discrete Architectural Surfaces by use of Circle Packing

Shizuo Kaji^a Jingyao Zhang^{b,*}

^a*Institute of Mathematics for Industry, Kyushu University, Japan*

^b*Dept. of Architecture and Architectural Engineering, Kyoto University, Japan*

Abstract

This paper presents an efficient approach for the conceptual design of architectural surfaces which are composed of triangular panels. Given an initial design, the proposed method finds a triangulated surface with user-specified Gaussian curvatures (not limited to constant Gaussian curvatures) while keeping some of the vertices fixed. In addition, the *conformal class* of the final design can be specified; that is, the user has control over the shape (the corner angles) of each triangular panel. The panels could be encouraged to form a regular tessellation or kept close to those of the initial design. This allows the free-form design of discrete architectural surfaces that achieve curvature requirements posed by stiffness and constructability. Furthermore, controllability on the conformal class suppresses possible distortion of the panels, resulting in higher structural performance and aesthetics.

Our method relies on the idea in discrete differential geometry called *circle packing*. In this line of research, the discrete Ricci flow has been widely used for surface modelling. However, it is not trivial to incorporate constraints such as boundary locations and convexity of the spanned surface, which are essential to architectural applications. Due to this difficulty, few concrete applications of the discrete Ricci flow have been reported which specifically aims at creation of architectural surfaces. We propose a perturbation of the discrete Ricci energy and develop a least-squares-based optimisation scheme to address these problems with a working implementation¹.

Key words: geometry processing; surface modelling; architectural surfaces; Gaussian curvature; circle packing.

¹ Our codes are publicly available at https://github.com/shizuo-kaji/ricci_flow

* Address: C2 Building, Kyotodaigaku-katsura, Nishikyo-ku, Kyoto, 615-8540, Japan. Tel/Fax: +81-(75)-383-2924 E-mail: zhang@archi.kyoto-u.ac.jp

1 Introduction

Upon the rapid development in digital technology, free-form surfaces have found their progressively important position in contemporary architecture. The advent of free-form surfaces makes geometry design more complex and challenging, leading to a new research area called *architectural geometry* [1]. Architectural geometry is an interdisciplinary research area lying on the border of differential geometry, computational geometry, and architectural design and engineering. Research in architectural geometry aims to develop new tools for the creation of digital models that meet practical and aesthetic requirements in architecture.

Most of the modern architectural surfaces are intrinsically discrete, with only a few exceptions that are truly continuous such as membrane and concrete shell structures. The geometry of discrete surfaces has been extensively studied in the field of *discrete differential geometry* (see [2] for a survey). Various techniques such as the mean curvature flow [3] and the Ricci flow [4] have been utilised in surface modelling. These methods formulate the problem of finding surfaces with specified design targets as variational problems with certain energy functionals.

In the design of architectural surfaces, among the design targets involving geometric property is the Gaussian curvature. In the past decades, double curvature structural envelopes (that is, non-developable surfaces) have become increasingly popular in architectural design due to their expressiveness and mechanical efficiency. It is, however, challenging to design such surfaces. One designing principle is to specify the boundary of the surface and a rough (expected) shape that spans the boundary, and rely on an algorithmic technique to find the final surface numerically. For example, a numerical form-finding method was presented based on the generation of linear Weingarten surfaces [5]. This method allows to build the surfaces on a target boundary curve but does not allow the user to specify the Gaussian curvatures of the interior vertices explicitly. Another method is proposed to obtain a surface with user-specified Gaussian curvatures based on the Gaussian curvature flow [6]. However, it is shown to be highly unstable. Furthermore, the shape of the panels could be distorted in the obtained surface even when the initial surface consists of near-regular panels. Keeping (regular) shapes of the panels is important to aesthetic appearance of the surface and to structural performance. To preserve the angles of the panels of the initial surface, Ricci flow-based methods have been developed [4,7,8,9], which find final surfaces *conformal* to the initial one (see [10] for a survey). However, existing applications of Ricci flow-based algorithms mainly focus on flattening surfaces to have the constant Gaussian curvatures at all vertices. This agrees with the fact that the Ricci flow is closely related to the uniformisation theorem [11]. Furthermore,

existing Ricci flow-based algorithms do not pay much attention to imposing constraints such as boundary locations and convexity (or concavity) of the resulting surface, which are relevant to architectural applications.

These problems in designing discrete architectural surfaces motivate us to present an efficient tool for quick conceptual design, which produces a surface with user-specified Gaussian curvatures and boundary vertex locations within a user-specified conformal class. Our flexible framework allows the user to incorporate other constraints as well. As an example, finding a convex surface with user-specified Gaussian curvatures is demonstrated.

After the introduction, this paper is organised as follows: Section 2 describes the background of discrete surfaces and circle packing on them. Section 3 discusses the algorithmic details of our method. Section 4 presents numerical examples to validate the proposed approach and demonstrate its versatility for the free-form design of discrete surfaces. Section 5 concludes the study with limitations of the proposed method and visions of future works.

2 Overview of discrete conformal surface geometry

This section provides an overview of the surface modelling based on discrete conformal geometry. We put a particular emphasis on various geometric structures on discrete surfaces and their hierarchy. Although we often use the terminology in differential geometry to evoke analogy, we do not rely on the knowledge of differential geometry, and we give a definition to each notion relevant in our setting.

2.1 Triangulated surface mesh

In this study, we consider surfaces that are triangulated meshes. An abstract triangulated mesh (a mesh, for short) is composed of the set \mathcal{V} of vertices, the set \mathcal{E} of edges, and the set \mathcal{F} of triangular faces. Here, we have architectural surfaces composed of triangular panels (faces) in mind. The edge connecting two vertices $i, j \in \mathcal{V}$ is denoted by e_{ij} , and the face formed by three vertices i, j , and k is denoted by f_{ijk} . As we are modelling surfaces, we always assume that the neighbourhood of each vertex is homeomorphic to the plane or the half-plane, and each edge is contained in at most two faces. An edge is said to be *interior* (resp. *boundary*) if it is contained in two faces (resp. a single face). The set of boundary edges is denoted by \mathcal{E}_{bd} . The vertices contained in boundary edges are called *boundary vertices*, and the set of boundary vertices is denoted by \mathcal{V}_{bd} .

A mesh is a combinatorial object and retains only the topology of the surface; that is, no information on lengths, areas, vertex positions are associated. The information on sizes can be bestowed by edge lengths $\ell : \mathcal{E} \rightarrow \mathbb{R}_{\geq 0}$; an assignment of non-negative number $\ell(e_{ij}) = l_{ij}$ for each edge e_{ij} . Since faces are triangles, we demand the edge lengths to satisfy the triangular inequality $l_{ij} + l_{jk} > l_{ik}$ for any face f_{ijk} . In this case, we say the edge lengths $\{l_{ij}\}$ define a *discrete Riemannian metric* (a metric, for short) on a mesh. Note that the edge lengths completely determine the shapes of the triangle faces, but not the dihedral angles between them (see Fig. 1).

The Gaussian curvature at a vertex quantifies the deviation of the neighbourhood of the vertex from a plane. There are several (non-equivalent) definitions of Gaussian curvatures for a mesh with a metric. In this paper, we adopt the angle defect as their definition. Namely, the Gaussian curvature K_i at vertex i is defined as follows:

$$\begin{aligned} K_i &= 2\pi - \sum_{f_{ijk} \in \mathcal{F}} \theta_i^{jk} & (i \notin \mathcal{V}_{\text{bd}}), \\ K_i &= \pi - \sum_{f_{ijk} \in \mathcal{F}} \theta_i^{jk} & (i \in \mathcal{V}_{\text{bd}}), \end{aligned} \quad (1)$$

where θ_i^{jk} is the corner angle at vertex i in the face f_{ijk} . The Gaussian curvatures of a mesh are computed solely from its metric independent of the coordinates of its vertices; such a geometric property is said to be *intrinsic*.

Although a metric determines the local shape of a mesh, its global realisation as a surface in space is not specified merely by a metric. An *embedding* $\psi : \mathcal{V} \rightarrow \mathbb{R}^3$ of a mesh assigns the coordinates $v_i = \psi(i) \in \mathbb{R}^3$ to each vertex $i \in \mathcal{V}$. Fig. 1 shows an example of two embeddings of a mesh with a metric. They have the same edge lengths, and hence, the same Gaussian curvatures.

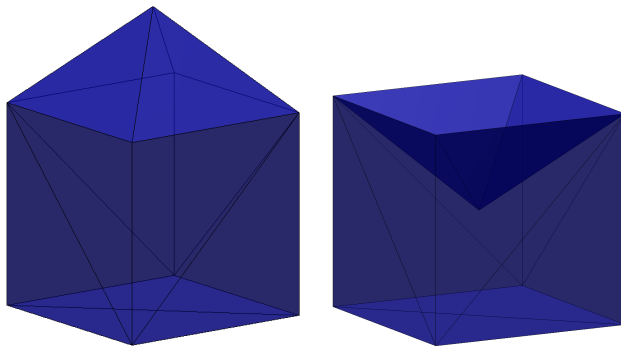


Fig. 1. Example of different embeddings of a mesh with a metric

2.2 Circle packing on a mesh

For smooth surfaces, conformal deformations are characterised as deformations that preserve angles. However, a general discrete surface represented by a triangulated mesh cannot be deformed to a non-similar one without changing the corner angles of the triangles. Obviously, we need more flexibility to design architectural surfaces. To avoid this rigidity (or locking) problem, we need a different notion of conformality in the discrete setting. There are several non-equivalent definitions of conformality of discrete surfaces (see [12] for a survey), we rely on Thurston’s idea [13] to look at *circle packing*. Under a conformal deformation of a smooth surface, the intersection angles of infinitesimal circles covering the surface do not change. In analogy, for a triangular mesh, we consider a circle packing in which a circle of finite radius $r_i > 0$ is assigned to each vertex i . Colloquially, a deformation is conformal if it does not alter the intersection angles of the circles (this analogy is made precise in [14]). The intersection angle (see Fig. 2(a)) ϕ_{ij} between the circles at vertices i and j is computed by:

$$\cos \phi_{ij} = \frac{l_{ij}^2 - r_i^2 - r_j^2}{2r_i r_j}, \quad (2)$$

where i and j are connected by an edge e_{ij} . *Thurston’s circle packing* of a mesh additionally assumes that the circles intersect with non-obtuse angles $\{\phi_{ij} \in [0, \pi/2]\}$. However, it is not easy to find Thurston’s circle packing in practice for a given mesh with a metric. Hence, we rely on a relaxed and abstract notion of *conformal structure* on a mesh, which is an assignment of $\eta_{ij} \geq 0$ for each edge e_{ij} . For a Thurston circle packing, we define $\eta_{ij} = \cos \phi_{ij}$. We also allow “non-intersecting” circle packing as in Fig. 2(b).

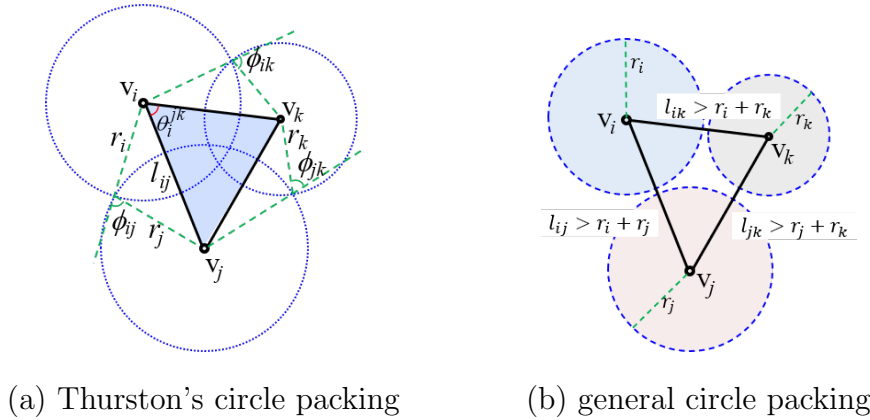


Fig. 2. Circle packing on a mesh.

For a mesh with a circle packing $\{r_i\}$ and a conformal structure $\{\eta_{ij}\}$, a metric

$\{l_{ij}\}$ can be associated by

$$l_{ij}^2 = r_i^2 + r_j^2 + 2r_i r_j \eta_{ij} \quad (\forall e_{ij} \in \mathcal{E}). \quad (3)$$

From this relation, a conformal structure together with a circle packing determines a metric. By rewriting the formula, we see a metric together with a circle packing determine a conformal structure analogously to (2):

$$\eta_{ij} = \frac{l_{ij}^2 - r_i^2 - r_j^2}{2r_i r_j}. \quad (4)$$

We define a *conformal deformation* of a mesh with a conformal structure $\{\eta_{ij}\}$ as a deformation that preserves the discrete conformal structure.

For a given mesh with a metric, there are several heuristic ways to define a circle packing radius r_i at vertex i from the metric. A popular choice [15] is given by

$$r_i = \frac{1}{2} \min_{f_{ijk} \in \mathcal{F}} (l_{ik} + l_{ij} - l_{jk}). \quad (5)$$

When an initial design is given as an embedded mesh, we can define its conformal structure by (4) and (5). Alternatively, we can ignore the initial design, and set $\eta_{ij} = 1$ for all $e_{ij} \in \mathcal{E}$, which would be the conformal structure of a regular tessellation.

2.3 Constraint on Gaussian curvature

The primary goal of this paper is to find an embedding of a mesh that achieves user-specified Gaussian curvatures. We would like to recall the fact that the Gaussian curvatures cannot take arbitrary values but are constrained by the mesh topology and geometry. First, the Gauss-Bonnet theorem imposes the topological constraint:

$$\sum_{i \in \mathcal{V}} K_i = 2\pi \chi(\mathcal{F}), \quad (6)$$

where

$$\chi(\mathcal{F}) = |\mathcal{V}| - |\mathcal{E}| + |\mathcal{F}| \quad (7)$$

is the Euler characteristic of the mesh. Second, the conformal structure imposes the geometric constraint [16,4]: For any proper subset $I \subset \mathcal{V}$,

$$\sum_{i \in I} K_i > - \sum_{(e_{jk}, i) \in Lk(I)} (\pi - \eta_{jk}) + 2\pi \chi(F_I), \quad (8)$$

where F_I is the set of the faces whose vertices are in I , and $Lk(I) = \{(e_{jk}, i) \in \mathcal{F} \mid i \in I, j, k \notin I\}$ is the link of I .

2.4 Metric deformation of a mesh

As a Riemannian metric determines the Gaussian curvatures of a smooth surface, a metric on a mesh (edge lengths) determines the corner angles of the triangular faces by cosine law, and in turn, the Gaussian curvatures of its vertices. To find a metric having the user-specified Gaussian curvatures, the Ricci flow can be utilised. The Ricci flow for discrete surfaces was established by [16] in analogy to its smooth counterpart introduced in [11]. It was shown that under a mild condition, the discrete Ricci flow converges quickly to give a metric having the specified Gaussian curvatures while preserving the conformal structure. As our method is closely related to the discrete Ricci flow, we give a brief description of it. We refer the reader to [10] for details of the discrete Ricci flow.

With a fixed mesh with a fixed discrete conformal structure, we are to find such a metric that gives a Gaussian curvature closed to a user-specified one \bar{K}_i at each vertex v_i . The key point is that we deform the circle radii instead of directly deforming the metric or the vertex positions. Recall that with a fixed conformal structure $\{\eta_{ij}\}$, the metric $\{l_{ij}\}$ is reconstructed by the circle radii $\{r_i\}$ by (3). The strategy of deforming the circle radii instead of the edge lengths has two advantages. First, one can specify the conformal class of the metric. Second, edge lengths obtained by (3) automatically satisfy triangular inequality so that we do not have to care the space of feasible solutions.

Denote the vector $(u_1, u_2, \dots, u_{|\mathcal{V}|})$ by \mathbf{u} , where $u_i = \ln r_i$. Given a prescribed Gaussian curvature \bar{K}_i for each vertex $i \in \mathcal{V}$, the Ricci energy is defined by

$$E(\mathbf{u}) = \int_{\mathbf{0}}^{\mathbf{u}} \sum_{i \in \mathcal{V}} (K_i(u) - \bar{K}_i) du_i = \int_{\mathbf{0}}^{\mathbf{u}} \sum_{i \in \mathcal{V}} K_i du_i - \sum_{i \in \mathcal{V}} \bar{K}_i u_i, \quad (9)$$

where $\mathbf{0} = (0, 0, \dots, 0)$ is the null vector. The integral does not depend on the path as the integrand can be shown to be an exact form. It is proved in [16] that when $\{\bar{K}_i\}$ satisfy (8), the Ricci energy is strictly convex on the space $\sum_{i \in \mathcal{V}} u_i = 0$, which amounts to fixing the indeterminacy of the uniform scaling. The discrete Ricci flow is the negative gradient flow of the Ricci energy, which is calculated as

$$\frac{d\mathbf{u}}{dt} = -\nabla E(\mathbf{u}) = (\bar{K}_1 - K_1(\mathbf{u}), \bar{K}_2 - K_2(\mathbf{u}), \dots, \bar{K}_{|\mathcal{V}|} - K_{|\mathcal{V}|}(\mathbf{u})). \quad (10)$$

Under the conditions (6) and (8), the Ricci energy attains its global minimum when $\nabla E(\mathbf{u}) = 0$, which means $K_i(\mathbf{u}) = \bar{K}_i$ for all $i \in \mathcal{V}$.

While the Ricci flow provides a powerful method for mesh deformation backed with a theoretical guarantee, the condition (8) is difficult to check in practice because the number of proper subsets $I \subset \mathcal{V}$ is exponential with respect to the number of vertices. In addition, while the gradient of the Ricci energy has a simple closed-form expression (10), its value itself is defined by an integral (9) and has no analytic closed-form expression. This hinders the use of most of modern optimisation techniques such as trust region which require the evaluation of the target function value. Our idea is to modify the Ricci energy so that it admits a closed, least-squares form, which allows us to use well-established solvers and to incorporate various constraints such as boundary positions and convexity. We propose the modified Ricci energy defined by

$$\hat{E}(\mathbf{u}) = \sum_{i \in \mathcal{V}_K} (K_i(\mathbf{u}) - \bar{K}_i)^2, \quad (11)$$

where $\mathcal{V}_K \subset \mathcal{V}$ is a subset of vertices on which we would like to specify their Gaussian curvatures (typically, the set of interior vertices is chosen). When $\{\bar{K}_i\}$ satisfy (6) and (8), the function $\hat{E}(\mathbf{u})$ attains the same global minimum as the Ricci energy (9), although we cannot assert that there are no other local minima. The gradient of (11) is easily computed using the formula for $\frac{\partial K_i}{\partial u_j}$ given, e.g., in [4].

Once the circle radius $r_i = \exp u_i$ for each vertex v_i is obtained by minimising (11), the edge lengths l_{ij} are computed by (3), while the discrete conformal structure $\{\eta_{ij}\}$ is kept unchanged from their initial values.

Remark 1 *There are different types of geometry (Euclidean, spherical, hyperbolic) for the circle packing on surfaces, and discrete Ricci flows are often introduced with general background geometry [4]. In this paper, we focus on Euclidean background geometry since our panels are triangles in Euclidean geometry.*

Table 1

Relation among structures

	mesh	metric	curvature	circle packing	conformal str.	embedding
symbol	$\mathcal{V}, \mathcal{E}, \mathcal{F}$	$\{l_{ij} \mid e_{ij} \in \mathcal{E}\}$	$\{K_i \mid i \in \mathcal{V}\}$	$\{r_i \mid i \in \mathcal{V}\}$	$\{\eta_{ij} \mid e_{ij} \in \mathcal{E}\}$	$\{v_i \in \mathbb{R}^3\}$
determined by		$\{v_i\}$, or $\{\eta_{ij}\}$ and $\{r_i\}$	$\{l_{ij}\}$	$\{l_{ij}\}$ (not canonical)	$\{l_{ij}\}$ and $\{r_i\}$	

3 Implementation of our method

In the previous section, we summarised how various properties are determined on the surface as functions of other properties. A mesh defines the topology and serves as a container of geometric structures. An embedding is a function $\psi : \mathcal{V} \rightarrow \mathbb{R}^3$ specifying the vertex coordinates $\{v_i \in \mathbb{R}^3 | i \in \mathcal{V}\}$. An embedding defines the metric, which is a function $\ell : \mathcal{E} \rightarrow \mathbb{R}$ specifying the edge lengths $\{l_{ij} \in \mathbb{R} | e_{ij} \in \mathcal{E}\}$. The shapes of the faces (triangle panels) and the Gaussian curvatures are solely determined by the metric independent of an embedding. On the other hand, a circle packing is a function $r : \mathcal{V} \rightarrow \mathbb{R}$ specifying the radius of a circle centred at each vertex. A conformal structure $\eta : \mathcal{E} \rightarrow \mathbb{R}$ is determined by the circle packing and the metric. In the opposite way, a conformal structure together with a circle packing determines a metric. Table 1 summarises the relations among various structures on a mesh.

When we would like to control a certain property, say the Gaussian curvature, we can deform upstream properties such as edge lengths and circle packing radii. This allows us flexibility in choosing design variables when the problem is formulated in terms of an optimisation problem.

Our proposed method consists of two steps; metric optimisation and embedding optimisation (see Fig. 3). Given a mesh and a conformal structure, the metric optimisation finds a metric $\{l_{ij}\}$ having the user-specified Gaussian curvatures and the user-specified lengths on a subset \mathcal{E}_{fix} of edges (typically, the set of the boundary edges). Then, the embedding optimisation finds an embedding $\{v_i \in \mathbb{R}^3\}$ having the metric $\{l_{ij}\}$ obtained in the previous step and the user-specified coordinates on a subset \mathcal{V}_{fix} of vertices (typically, the set of the boundary vertices). The final design is obtained as the embedded mesh in the Euclidean 3-space \mathbb{R}^3 .

3.1 Metric optimisation

Assume that a mesh $(\mathcal{V}, \mathcal{E}, \mathcal{F})$ together with user-specified target Gaussian curvatures $\{\bar{K}_i | i \in \mathcal{V}_K\}$ on a subset \mathcal{V}_K of vertices (typically, the set of interior vertices) is given. Moreover, the user specifies a conformal structure $\{\eta_{ij}\}$. For example, if the mesh has a uniform vertex valence of six, setting the constant value $\eta_{ij} = 1$ for all edges $e_{ij} \in \mathcal{E}$ encourages the final mesh to have a regular tessellation with equilateral triangular panels. Alternatively, if an initial design is given, the conformal structure η_{ij} can be computed from its metric by (5) and (4). In this case, the final mesh will be in the same conformal class as the initial one, and hence, the shape of panels are expected to be preserved. Moreover, the user can specify certain edges $e_{ij} \in \mathcal{E}_{\text{fix}}$ to have

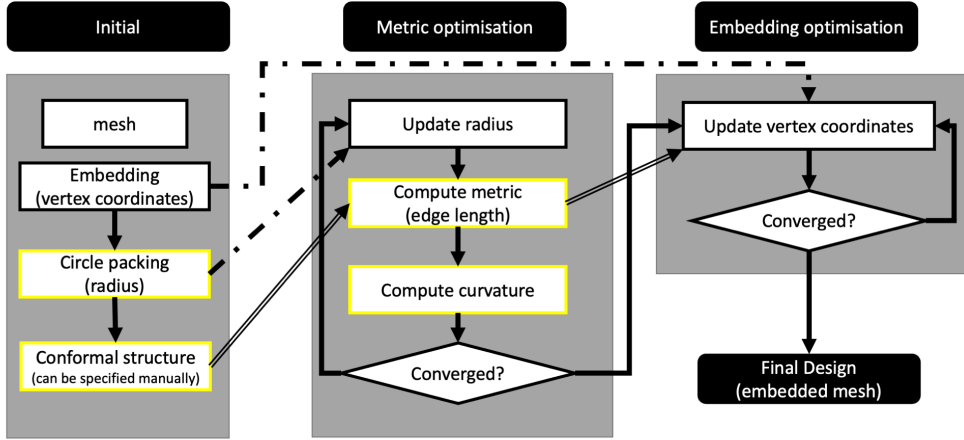


Fig. 3. Overview of the proposed method. The dashed arrows indicate the values are used as the initial solution. The double-line arrows indicate the values are used but not changed.

the specified lengths \bar{l}_{ij} :

$$l_{ij} = \bar{l}_{ij} \quad (e_{ij} \in \mathcal{E}_{\text{fix}}).$$

For example, if we would like the positions of the boundary vertices fixed to $\{\bar{v}_i \mid i \in \mathcal{V}_{\text{bd}}\}$ in the final embedding, we set $\mathcal{E}_{\text{fix}} = \mathcal{E}_{\text{bd}}$ and $\bar{l}_{ij} = |\bar{v}_i - \bar{v}_j|$ at this stage.

To achieve these goals, we solve the following non-linear least-squares problem:

$$\begin{aligned} & \text{Find} && u_i, && (i \in \mathcal{V}) \\ & \text{Minimize} && \sum_{i \in \mathcal{V}_K} (K_i(\mathbf{u}) - \bar{K}_i)^2 + \lambda_e \sum_{e_{ij} \in \mathcal{E}_{\text{fix}}} (l_{ij}(\mathbf{u})^2 - \bar{l}_{ij}^2)^2, && (12) \end{aligned}$$

where the first term is the modified Ricci energy (11), and $l_{ij}(\mathbf{u})$ is computed by (3) and $r_i = \exp u_i$. The hyper-parameter $\lambda_e \geq 0$ controls the trade-off between conformity to the specified Gaussian curvature and the specified edge lengths. Once u_i are obtained as the solution to (12), the metric $\{l_{ij}\}$ is computed by (3) with $r_i = \exp(u_i)$.

Remark 2 *Instead of u_i , we can directly optimise the radii r_i in (12). The variable u_i is often called the conformal factor in analogy to the smooth setting. Algorithmically, setting $r_i = \exp(u_i)$ serves as a change of variables to ensure the positivity constraint $r_i > 0$. We may also directly optimise the edge lengths l_{ij} since K is a function of l_{ij} as well. However, we cannot specify the conformal class of the resulting metric. Moreover, ensuring the triangular inequality can be problematic. Our codes implement all these choices; u_i , r_i , and l_{ij} .*

3.2 Embedding optimisation

Now, we would like to find an embedding $\{v_i \in \mathbb{R}^3\}$ of the mesh which realises the metric $\{l_{ij}\}$ obtained in the previous step while a subset \mathcal{V}_{fix} of vertices (typically, the boundary vertices) have the user-specified coordinates

$$v_i = \bar{v}_i \quad (i \in \mathcal{V}_{\text{fix}}).$$

The embedded mesh is the final design we would like to obtain. The problem is similar to the classical multi-dimensional scaling (MDS) [17] in which an embedding of finite points with a specified distance matrix is sought for. Our embedding problem can be thought of as a generalisation of MDS to graphs where only a subset of pairs have specified distances. This is a type of *graph embedding* problem [18]. What is peculiar to our case is the fact that a uniform scaling will not change the Gaussian curvatures at the vertices. Hence, we introduce a scaling factor $\beta > 0$ and solve the following non-linear least-squares problem²:

$$\begin{aligned} & \text{Find} && \beta, v_i, && (i \in \mathcal{V}) \\ & \text{Minimize} && \sum_{e_{ij} \in \mathcal{E}} (|v_i - v_j|^2 - \beta l_{ij}^2)^2 + \lambda_v \sum_{i \in \mathcal{V}_{\text{fix}}} |v_i - \bar{v}_i|^2, && (13) \end{aligned}$$

where $\lambda_v \geq 0$ is a hyper-parameter controlling the trade-off between conformity of the Gaussian curvature and the boundary coordinates. Other constraints can be easily incorporated by adding penalty terms to (13). For example, to enforce the convexity at internal vertices, we add the following term with a hyper-parameter $\lambda_c \geq 0$

$$\lambda_c \sum_{i \in \mathcal{V} \setminus \mathcal{V}_{\text{bd}}} f(\tilde{v}_{i,z} - v_{i,z}), \quad \left(f(x) = \frac{x}{1 + \exp(-x)} \right), \quad (14)$$

where $v_{i,z}$ is the z -coordinate of v_i and $\tilde{v}_{i,z}$ is the mean of the z -coordinates of the vertices adjacent to v_i . The sigmoid-weighted linear function [19] $f(\tilde{v}_{i,z} - v_{i,z})$ penalises $\tilde{v}_{i,z} - v_{i,z}$ to have positive values, and its gradient is computed by $f'(x) = f(x) + \frac{1 - f(x)}{1 + \exp(-x)}$.

If an initial design is given as an embedded mesh, its vertex positions are used as the initial solution for the optimisation problem (13). Note that finding an embedding which realises the specified metric is not convex, and there can be multiple global minima, as is seen in Fig. 1. In this case, the choice of an initial solution affects the final solution.

² When $\mathcal{V}_{\text{fix}} = \emptyset$, we set $\beta = 1$ and do not optimise β to avoid the degenerate solution of $\beta = 0$ and $v_i = v_j$ for all $i, j \in \mathcal{V}$

There exists a metric for a mesh with a conformal structure which realises the specified Gaussian curvature if and only if (6) and (8) are satisfied. Furthermore, when such a metric exists, it is unique up to a uniform scaling. However, there may not exist an embedding which realises the metric [20]. Also, there can be multiple non-congruent embeddings which realise the metric. Therefore, the metric optimisation is theoretically more troublesome, and this part is separated from the whole procedure in our scheme.

3.3 Numerical examples

In this section, we present several numerical examples to validate the proposed method. In Examples 1, 2, and 4, we consider the design of surfaces with constant Gaussian curvature (CGC), while in Example 3, we present a surface with non-uniform curvature, having both positive and negative values, to demonstrate the design flexibility of the proposed method. The Euler characteristic number for the surfaces in all examples is 1, and hence, the total Gaussian curvature of the surface is 2π by the Gauss-Bonnet theorem (6).

We evaluate the results in terms of the mean absolute errors of the Gaussian curvatures, the coordinates of the boundary vertices, and the angles of the faces between the target values and the final embedded mesh:

$$\begin{aligned}
 A_K &= \frac{1}{|\mathcal{V}_K|} \sum_{i \in \mathcal{V}_K} |K_i - \bar{K}_i|, \\
 A_v &= \frac{1}{|\mathcal{V}_{\text{fix}}|} \sum_{i \in \mathcal{V}_{\text{fix}}} |v_i - \bar{v}_i|, \\
 A_\theta &= \frac{1}{3|\mathcal{F}|} \sum_{f_{ijk} \in \mathcal{F}} \left(|\theta_i^{jk} - \bar{\theta}_i^{jk}| + |\theta_j^{ki} - \bar{\theta}_j^{ki}| + |\theta_k^{ij} - \bar{\theta}_k^{ij}| \right), \quad (15)
 \end{aligned}$$

where $\bar{\theta}_i^{jk}$ are the target corner angles of the triangular panels, and θ_i^{jk} are those of the final mesh. When a conformal structure is given by an initial design, $\bar{\theta}_i^{jk}$ are the corner angles of the initial mesh. When a conformal structure is specified manually, $\bar{\theta}_i^{jk}$ depends on the mesh topology.

All the experiments are performed by our Python script³ using SciPy optimisers [21]. There is a trade-off among above-mentioned evaluation indicators. We can control the trade-off by modifying the hyper-parameters such as λ_e , λ_v , and stopping criteria for optimisation. We terminate the optimisation steps when the norm of the gradient gets less than 10^{-6} . Timing is measured on a MacBook Pro with a M1 core using a single core. The results are summarised in Table 2.

³ https://github.com/shizuo-kaji/ricci_flow

Table 2

Error analysis and computation time of examples

	A_K (radian)	A_v (meter)	A_θ (degrees)	metric opt. (sec)	embedding opt. (sec)
Ex1a	1.37×10^{-4}	8.09×10^{-2}	0.49	0.28	0.32
Ex1b	6.07×10^{-5}	1.96×10^{-2}	0.99	0.28	0.55
Ex1c	9.12×10^{-6}	6.80×10^{-3}	0.13	0.60	0.26
Ex1d	1.72×10^{-2}	6.52×10^{-4}	0.55	0.33	0.31
Ex2a	3.73×10^{-4}	8.64×10^{-2}	1.23	0.25	0.59
Ex2b	1.09×10^{-3}	0.117	0.25	0.47	0.96
Ex3	4.24×10^{-4}	8.31×10^{-2}	0.54	0.24	1.87
Ex4a	2.09×10^{-3}	0.183	0.49	0.28	1.00
Ex4b	3.92×10^{-4}	4.86×10^{-2}	0.46	0.28	1.09

Example 1: CGC surface with a hexagonal plan

In this example, we consider a constant Gaussian curvature (CGC) surface with a hexagonal plan. The initial geometry is shown in Fig. 4. Its span is 30.0m and its height is 10.0m. This surface is composed of 169 vertices (of which 42 are boundary vertices), 462 edges, and 294 faces.

For comparison, we performed several experiments with the same mesh but varying one design target at a time.

- For Ex1a, we set $\eta_{ij} = 1$ aiming at equilateral panels (that is, $\bar{\theta}_i^{jk} = \pi/3$). The total target Gaussian curvature for interior vertices is set to 1.5, and hence, the target Gaussian curvature \bar{K}_i of each interior vertex is 0.011811. The target positions of the boundary vertices are set to the same as in the initial geometry with $\lambda_v = \lambda_e = 0.01$.
- In Ex1b, the total target Gaussian curvature for interior vertices is set to 3.0, and hence, the target Gaussian curvature \bar{K}_i of each interior vertex is 0.023622. Other conditions are the same as Ex1a.
- In Ex1c, we calculate η_{ij} from the initial geometry by (5) and (4) so that the final mesh has similar triangle panels as the initial ones. Other conditions are the same as Ex1a.
- In Ex1d, we set $\lambda_v = \lambda_e = 100$ to stress the position condition of the boundary vertices. Other conditions are the same as Ex1a.

The final geometries are shown in Fig. 5. The distributions of the Gaussian curvatures and the corner angles at interior vertices for the initial and final meshes are shown in the violin plots [22] in Fig. 6 and 7.

In Ex1a, Ex1b, and Ex1c, the distributions of the Gaussian curvatures concen-

trate around the target values. In Ex1d, the stringent constraint increased the precision of the boundary location but this is achieved at a large cost of the precision of the Gaussian curvatures. This suggests that methods which only allow the user to specify the exact boundary locations will fail. Our method offers control over the trade-off through the choice a hyper-parameter.

In the initial geometry, the corner angles of the panels range from 50 to 70 degrees, while in Ex1a, Ex1b, and Ex1d, they are corrected to 60 degrees within 3 degrees of margins, resulting in a near regular tessellation in the final geometry. On the other hand, in Ex1c, the distribution of the corner angles is close to that of the initial geometry as desired.

Example 2: CGC surface with a square plan

We consider a CGC surface with a square plan as shown in Fig. 8. Its span is 30.0m, while its height is 6.0m. The surface is composed of 181 vertices (of which 36 are boundary vertices), 504 edges, and 324 triangle panels. The total target Gaussian curvature for interior vertices is set to 1.0, and hence, the target Gaussian curvature \bar{K}_i of each interior vertex is 6.897×10^{-3} . The target positions of the boundary vertices are set to the same as in the initial geometry with $\lambda_v = \lambda_e = 0.01$.

For the conformal structure, for Ex2a, we calculate η_{ij} from the initial geometry by (5) and (4) so that the final mesh has similar panel shapes as the initial ones. For Ex2b, we set the constant value $\eta_{ij} = 1$, aiming at isosceles right-angled triangle panels (that is, $\bar{\theta}_i^{jk} = \pi/2, \pi/4$).

The final geometry is shown in Fig. 8. The distributions of the Gaussian curvatures and the corner angles at interior vertices for the initial and final meshes are shown in Fig. 10 and 11.

The precision of the Gaussian curvature is worse in Ex2b than in Ex2a. This is because the target Gaussian curvatures violate (8) and cannot be realised with the regular tessellation and the boundary constraints.

Example 3: surface with non-uniform Gaussian curvature

In Example 3, we are to design a surface with varied target Gaussian curvatures taking positive values at some vertices and negative values at the others. The initial geometry of Example 1 is used in this example. We set $\eta_{ij} = 1$ aiming at equilateral panels (that is, $\bar{\theta}_i^{jk} = \pi/3$). The target Gaussian curvatures

are assigned by a quadratic curve defined as follows:

$$\begin{aligned} d_i &= -\frac{\sqrt{(x_i - x_0)^2 + y_i^2}}{2x_0}, \quad (0 \leq d_i \leq 1) \\ \bar{K}_i &= -\frac{2c}{b^2}(d_i - b)^2 + c, \quad (i \in \mathcal{V} \setminus \mathcal{V}_{\text{bd}}), \end{aligned} \quad (16)$$

where (x_i, y_i) are the (x, y) -coordinates of the initial embedding, and $c = 0.0168$, $b = 0.7$, and $x_0 = -12.86$. The target Gaussian curvature attains the maximum value c at $d_i = b$, and the minimum value $-c$ at $d_i = 0$. The total target Gaussian curvature of the interior vertices is 1.5. The target positions of the boundary vertices are set to the same as in the initial geometry with $\lambda_v = \lambda_e = 0.01$. Fig. 12 shows the final geometry of the surface. The distributions of the Gaussian curvatures and the corner angles at interior vertices for the final meshes are shown in Fig. 13 and 14.

Example 4: convex and non-convex final geometry

In Example 4, we are concerned with convexity. The initial geometry is shown in Fig. 15. Its span is 30.0m, while its height is 0.57m. This example is similar to Example 1 but with different boundary locations.

We have two variations of Example 4. For Ex4a, we set $\eta_{ij} = 1$. The total target Gaussian curvature for interior vertices is set to 1.5, and hence, the target Gaussian curvature \bar{K}_i of each interior vertex is 0.011811. The target positions of the boundary vertices are set to the same as in the initial geometry with $\lambda_v = \lambda_e = 0.01$. The obtained final geometry is non-convex, as shown in Fig. 16 (a).

For Ex4b, we add the convexity term (14) with $\lambda_c = 1.0$ to (13). Other conditions are the same as Ex4a. The final geometry is a convex surface, as shown in Fig. 16 (b).

The distributions of the Gaussian curvatures and the corner angles at interior vertices for the initial and the final meshes are shown in Fig. 13 and 14.

4 Conclusions

In this study, we presented an efficient tool for the design of discrete architectural surfaces having the user-specified Gaussian curvatures and boundary locations while providing control over the shape of the panels through the choice of the conformal class. The proposed method is composed of two successive optimisation procedures: the metric optimisation using a modified Ricci

energy and the embedding optimisation to realise the obtained metric. Both are formulated as least-squares problems, and any standard solvers can be used thanks to the closed-form expression of the modified Ricci energy. This formulation and the “change of the variables” in the optimisation problems are the key ideas of the proposed method. Instead of taking vertex coordinates directly as variables, the circle packing radii are chosen first as variables to find a metric. Then, vertex coordinates are used as variables to achieve the obtained metric. These ideas have led to our fast and robust algorithm. In addition, our method offers flexibility in incorporating various design constraints as penalty terms in the least-squares problem. Our implementation is publicly available as open-source and can be easily extended with additional penalty terms and different solvers.

One limitation of the proposed method is that only triangulated mesh can be handled due to the lack of the theory of conformal geometry for general polyhedral meshes. This limitation will be addressed in future work. Another challenging topic of future work is extending the present scheme to parametric surfaces such as NURBS surfaces.

Acknowledgement: This work was supported by JST CREST Grant Number JPMJCR1911. The authors are grateful to Prof. Makoto Ohsaki at Kyoto University for his helpful comments, and in particular, for providing Example 4.

References

- [1] H. Pottmann, Architectural geometry as design knowledge, *Architectural Design* 80 (4) (2010) 72–77. doi:10.1002/ad.1109.
- [2] K. Crane, Conformal geometry of simplicial surfaces, in: K. Crane (Ed.), *An Excursion Through Discrete Differential Geometry*, Proceedings of Symposia in Applied Mathematics, American Mathematical Society, 2020, pp. 59–102.
- [3] U. Pinkall, K. Polthier, Computing discrete minimal surfaces and their conjugates, *Experimental Mathematics* 2 (1) (1993) 15–36. doi:em/1062620735.
- [4] M. Jin, J. Kim, F. Luo, X. Gu, Discrete surface Ricci flow, *IEEE Transactions on Visualization and Computer Graphics* 14 (5) (2008) 1030–1043.
- [5] X. Tellier, C. Douthe, L. Hauswirth, O. Baverel, Linear Weingarten surfaces for conceptual design, *Proceedings of the International Symposium on Conceptual Design of Structures* (2019) 225–232.

- [6] H. Zhao, G. Xu, Triangular surface mesh fairing via Gaussian curvature flow, *Journal of Computational and Applied Mathematics* 195 (1-2) (2006) 300–311. doi:10.1016/j.cam.2005.03.094.
- [7] Y. L. Yang, R. Guo, F. Luo, S. M. Hu, X. Gu, Generalized discrete Ricci flow, *Computer Graphics Forum* 28 (7) (2009) 2005–2014. doi:10.1111/j.1467-8659.2009.01579.x.
- [8] M. Zhang, R. Guo, W. Zeng, F. Luo, S. T. Yau, X. Gu, The unified discrete surface Ricci flow, *Graphical Models* 76 (5) (2014) 321–339. doi:10.1016/j.gmod.2014.04.008.
- [9] M. Jin, X. Gu, Y. He, Y. Wang, *Conformal Geometry: Computational Algorithms and Engineering Applications*, Springer International Publishing, Cham, 2018. doi:10.1007/978-3-319-75332-4.
- [10] W. Zeng, X. D. Gu, *Ricci Flow for Shape Analysis and Surface Registration. Theories, Algorithms and Applications*, Springer, 2013. doi:10.1007/978-1-4614-8781-4.
- [11] R. Hamilton, The Ricci flow on surfaces, *Contemporary Mathematics* 71 (1988) 237–262.
- [12] K. M. Crane, *Conformal geometry processing*, Ph.D. thesis, California Institute of Technology, an optional note (2013). doi:doi:10.7907/8V9Z-N286.
- [13] W. P. Thurston, *Geometry and topology of 3-manifolds*, Princeton University, 1980.
- [14] B. Rodin, D. Sullivan, The convergence of circle packings to the Riemann mapping, *Journal of Differential Geometry* 26 (2) (1987) 349–360. doi:10.4310/jdg/1214441375.
- [15] P. L. Bowers, K. Stephenson, *Uniformizing Dessins and Belyi Maps Via Circle Packing*, American Mathematical Society, 2004.
- [16] B. Chow, F. Luo, Combinatorial Ricci flows on surfaces, *Journal of Differential Geometry* 63 (1) (2003) 97–129. doi:10.4310/jdg/1080835659.
- [17] A. Mead, Review of the Development of Multidimensional Scaling Methods, *The Statistician* 41 (1) (1992) 27. doi:10.2307/2348634.
- [18] H. Cai, V. W. Zheng, K. Chang, A comprehensive survey of graph embedding: problems, techniques and applications, *IEEE Transactions on Knowledge and Data Engineering* (2018).
- [19] S. Elfving, E. Uchibe, K. Doya, Sigmoid-weighted linear units for neural network function approximation in reinforcement learning, *Neural Networks* 107 (2018) 3–11, special issue on deep reinforcement learning. doi:https://doi.org/10.1016/j.neunet.2017.12.012.
- [20] P. Erdős, M. Simonovits, On the chromatic number of geometric graphs, *Ars Combin* 9 (1980) 229–246.

- [21] P. Virtanen, R. Gommers, T. E. Oliphant, et al., SciPy 1.0: fundamental algorithms for scientific computing in Python, *Nature Methods* 17 (3) (2020) 261–272. doi:10.1038/s41592-019-0686-2.
- [22] J. L. Hintze, R. D. Nelson, Violin Plots: A Box Plot-Density Trace Synergism, *Statistical computing and graphics* 52 (2) (1998) 181–184.

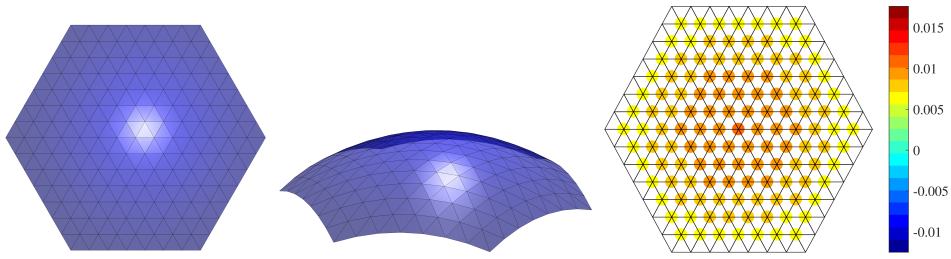


Fig. 4. Initial geometry of Example 1. From left to right: top view, perspective view, Gaussian curvatures.

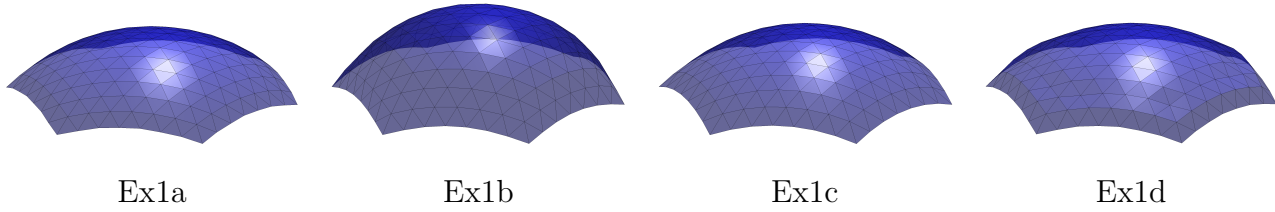


Fig. 5. Final geometry of Example 1.

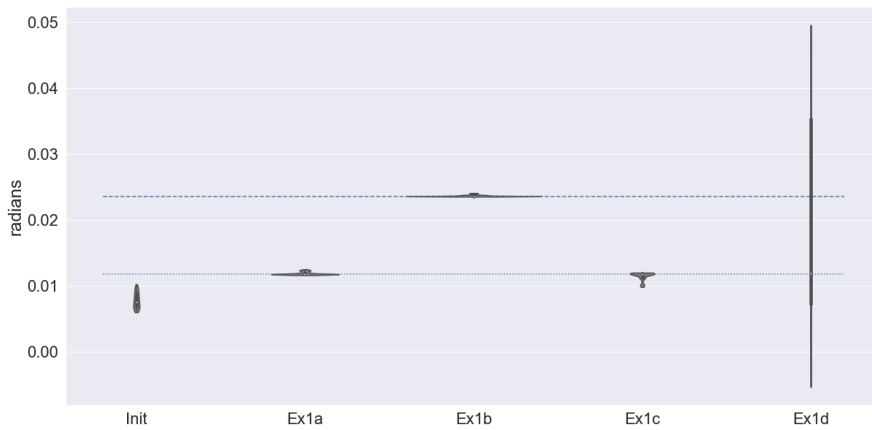


Fig. 6. Distribution of Gaussian curvature of Example 1. Target curvatures are set to $\bar{K}_i = 0.011811$ (dotted line) for Ex1a, Ex1c, and Ex1d, and $\bar{K}_i = 0.023622$ (dashed line) for Ex1b.

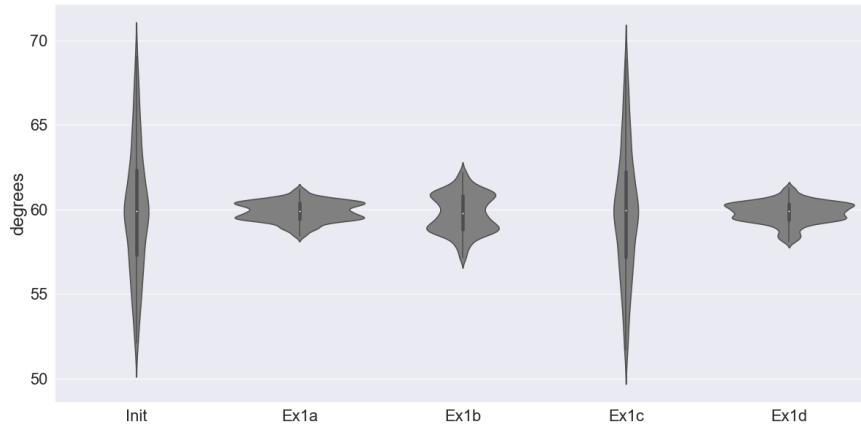


Fig. 7. Distribution of angles of Example 1. Target angles are set to 60 degrees for Ex1a, Ex1b, and Ex1d while they are set to the ones in the initial mesh in Ex1c.

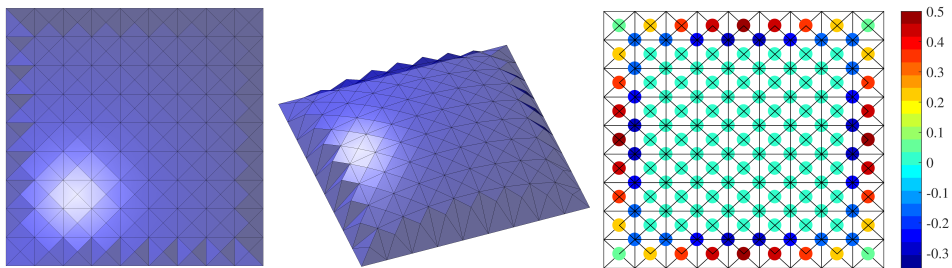


Fig. 8. Initial geometry of Example 2. From left to right: top view, perspective view, Gaussian curvatures.

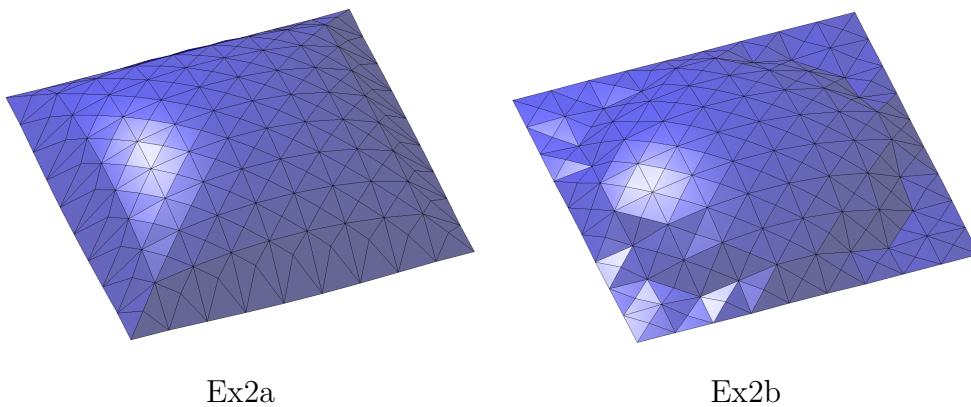


Fig. 9. Final geometry of Example 2.

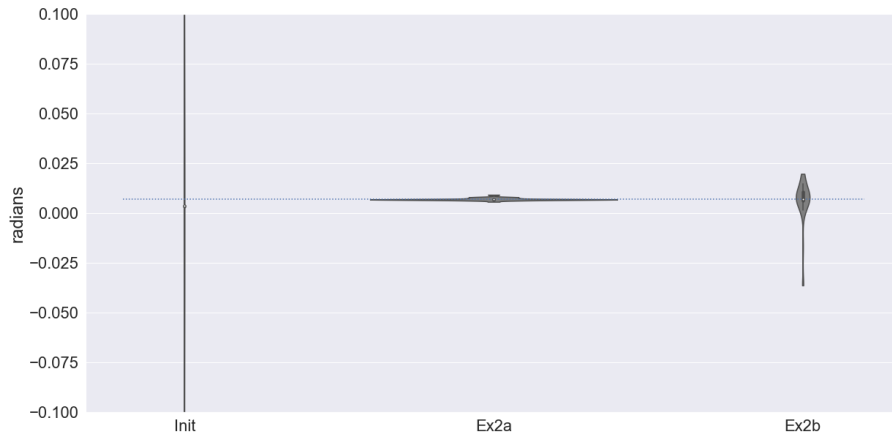


Fig. 10. Distribution of Gaussian curvature of Example 2. Target curvatures are set to $\bar{K}_i = 6.897 \times 10^{-3}$ (dotted line).

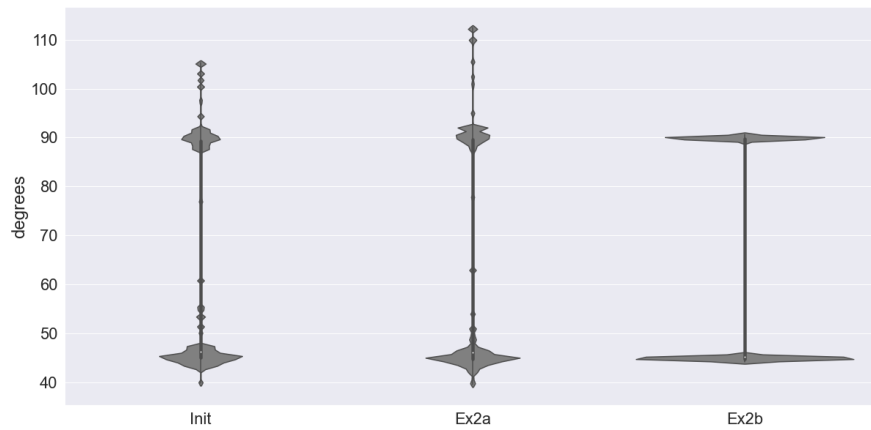


Fig. 11. Distribution of angles of Example 2. Target angles are set to the ones in the initial mesh for Ex2a, and to the ones in the regular tessellation (45 and 90 degrees) for Ex2b.

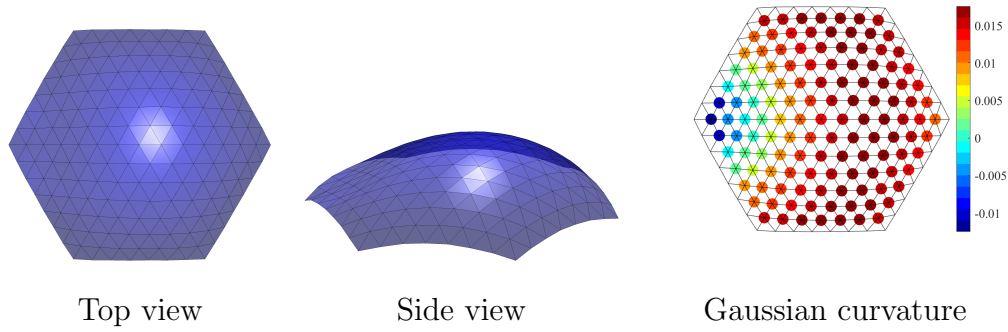


Fig. 12. Final geometry of Example 3.

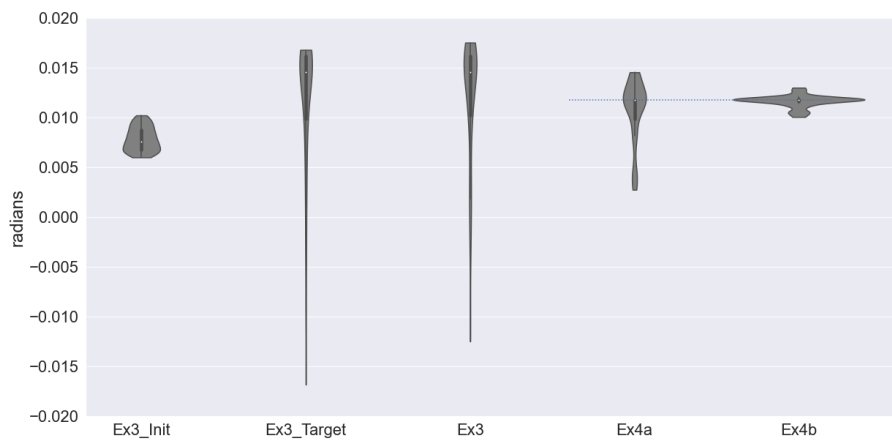


Fig. 13. Distribution of Gaussian curvature of Example 3 and 4. Target curvatures are set to $\bar{K}_i = 0.011811$ (dotted line) for Ex4a and Ex4b.

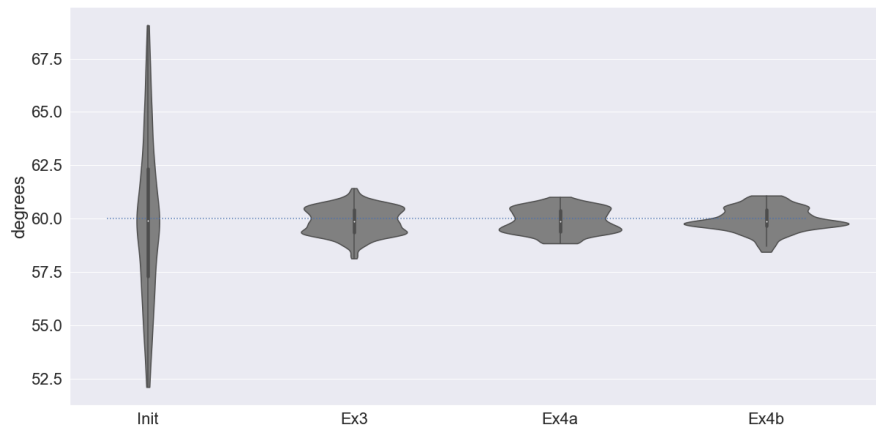


Fig. 14. Distribution of angles of Example 3 and 4. Target angles are set to 60 degrees.

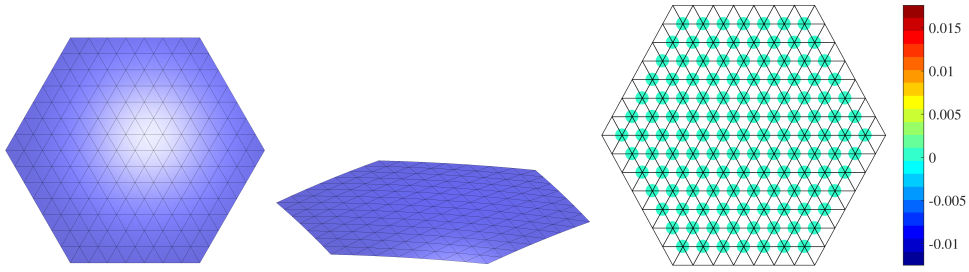


Fig. 15. Initial geometry of Example 4. From left to right: top view, perspective view, Gaussian curvatures.

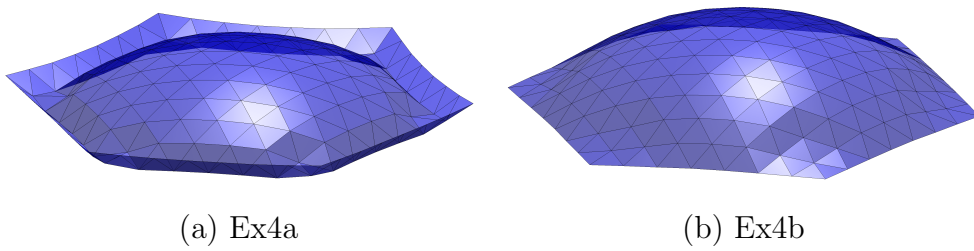


Fig. 16. Final geometry of Example 4.